Supervised Hierarchical Bayesian Model-Based Electomyographic Control and Analysis

Hyonyoung Han and Sungho Jo, *Member, IEEE*

***Abstract*—This work suggests a supervised hierarchical Bayesian model for surface electromyography (sEMG)-based motion classification and its strategy analysis. The proposed model unifies the optimal feature extraction and classification through probabilistic inference and learning by identifying the latent neural states (LNSs) that govern a collection of sEMG signals. In addition, the inference step provides an approach to identify distinct muscle activation strategies according to sEMG patterns based on LNSs. To validate the model, nine-class classification using four sEMG sensors on the limb motions is tested. The model performance is evaluated with relatively high and low activation levels, generalized classification across subjects and online classification. The model, based on LNSs to capture various motions, is assessed with respect to activation levels, individual subjects and transition during online classification. Our approach cannot only classify sEMG patterns, but also provide the interpretation of sEMG strategic patterns. This work supports the potential of the proposed model for sEMG control-based applications.**

***Index Terms*—Classification, electromyographic control, surface electromyography (sEMG), supervised hierarchical Bayesian model.**

I. Introduction

SURFACE electromyography (sEMG)-based muscle activation observation has been of particular interest as a noninvasive method for control [1]. This method has potential for applications in prosthetics [2]–[5], exoskeletons [6]–[9], robotics [10], [11], etc., and has been verified through various research results. While testing various algorithms to extract desired commands from encoded sEMG signals, the following popular algorithms have been explored in detail: neural networks [12], [13], fuzzy systems [5], [6], and the Hill-type muscle model [7], [8].

Artificial neural networks (ANNs) are one of the most popular machine learning-based classification and regression algorithms. ANNs enable prediction without a detailed model of the underlying musculoskeletal system. Conversely, they do not provide an explicit physical representation of the mechanism. Taking into account the fact that the human body is a complicated fuzzy system, a neurofuzzy algorithm for myoelectric control or interface has been proposed, especially for robotic exoskeleton applications [6]. A hierarchical neurofuzzy [14] controller has been found to be good adapting to people who generate different muscle activity levels. The Hill-type muscle model [15] explains the neurophysiological mechanism of muscle operation. A problem of the model-based approach is that the number of model parameters to be determined increases as more muscles are incorporated into the model, and the model parameters are subject dependent [16], [17]. In addition to the aforementioned approaches, onset analysis and finite state machine approaches have also been suggested [18].

Recently, there have been some attempts to apply Bayesian approaches for electromyographic control [19]–[22]. Especially, the hidden Markov model (HMM) [21] and the Gaussian mixture model (GMM) [22] have been applied for multiple limb motion classification using myoelectric signals. Bayesian approaches are generally known to be good at achieving an automatic and adaptive process without concrete information about the parameters and at incorporating prior information as well. On the other hand, they typically involve high-dimensional integrals. However, the recent advent of sufficient computational power and good methodology has made Bayesian approaches very attractive for solving complex problems.

Even though a variety of methods have been attempted so far, achieving a robust algorithm is still challenging because sEMG signals are very likely affected by a person's condition and the task performed. For classification and analysis of motions, generative model approaches may have advantages to provide an intuitive mechanism and to comprehensively describe the overall processing. Moreover, the sEMG strategies, which indicate an essential characteristic of sEMG executing a specific motion, could be different across subjects or differ in activation levels while executing similar motions. Therefore, a comprehensive model which can take into account individual strategies as well as classify signal patterns is expected to provide better results for extensive applications.

This paper proposes a new hierarchical Bayesian model to interpret a generation of a multitime series of sEMG data and classify the sEMG profiles (time series of each channel sEMG signal) into several classes. The proposed model assumes the probabilistic distribution of latent neural state (LNS) variables that infer sEMG profiles. By constructing a generative probabilistic model, probabilistic relationships among a set of latent intention variables are formed and possible sequences of sEMG

Manuscript received April 24, 2013; revised July 31, 2013 and September 24, 2013; accepted September 30, 2013. Date of publication October 4, 2013; date of current version June 30, 2014. This work was supported by the Agency for Defense Development of Korea under Grant UD1100511D, by the Korean Government (MTIE) under the Human Resources Development Program for Convergence Robot Specialists H1502-13-1001, and by the Korean Government (ME) under the Basic Science Research Program under Grant 2013R1A1A2009378.

The authors are with the Department of Computer Science, Korea Advanced Institute of Science and Technology, Daejeon, Korea (e-mail: hhn98@kaist.ac.kr; shjo@kaist.ac.kr).

Color versions of one or more of the figures in this paper are available online at http://ieeexplore.ieee.org.

Digital Object Identifier 10.1109/JBHI.2013.2284476

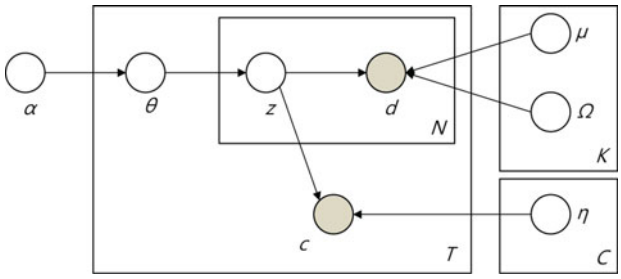

Fig. 1. Graphical model representation for the proposed supervised hierarchical Bayesian model. Each node is labeled according to its role in the generative process. Observed nodes indicating data d and label c are shaded while the other nodes indicating Dirichlet parameter α, Gaussian multimodal parameters μ and Ω, class coefficient parameter η, multinomial distribution of LNSs θ, and specific LNS z are unshaded.

data are generated based on the relationships. The probabilistic structure of the LNS variables makes it possible to classify activations from a set of sEMG profiles and to distinguish the sEMG motion strategies.

II. Supervised Hierarchical Bayesian Process Model for an sEMG-Based Classification

A. Motivation

The proposed model is motivated by Latent Dirichlet Allocation (LDA), which is the simplest topic model. LDA is based on the intuition that documents, which are sets of words, exhibit multiple topics [23]–[25]. LDA models document collections that are produced from latent topics by representing each topic as a distribution over a fixed vocabulary. The proposed model interprets the intuition behind the topic model with respect to a collection of sEMG profiles. It is proposed that we should regard an sEMG signal profile over time as a sequence of data units. An sEMG data unit, corresponding to a word in the topic model, contains features that play roles in the basic representation of data. Then, a trial, which records sEMG signals from multiple electrode channels, is a collection of a sequence of units. Assuming there are LNSs comparable to latent topics in the topic model, the trials are represented by random mixtures over latent intentions, in which each LNS is characterized by a distribution over data units. This work also proposes to use the Gaussian distribution to represent each LNS by taking into account the general features of sEMG signals [26], [27]. For applications to control, the model includes a classification procedure. The most likely classes are successively selected by assuming that a trial is associated with a sequence of intentions. The selected class labels can be interpreted as commands to an object intended to be controlled such as a robot, a prosthetic device, a wheelchair and so on.

B. Generative Process Model

A simple illustration of the proposed model is shown in Fig. 1. Suppose that training data are collected in T trials for C class classification, and a data sequence is made up of N data units in each trial (see Section II-C). Under the assumption that the number of LNSs, K, are fixed, the proposed model describes a generative process of data acquired at the dth trial, as follows:

1) Sample $\theta_d \sim \text{Dirichlet}\,(\alpha)$.
2) For each of the sEMG data units $(n = 1, \ldots, N)$, Sample $z_n \sim \text{Multinomial}\,(\theta_d)$. Sample $d_n \sim p(d_n|z_n, \mu_{1:K}, \Omega_{1:K})$ from a multivariate Gaussian distribution conditioned on z_n.
3) Sample $c \sim p(c|\overline{z}, \eta_{1:L})$ which represents a softmax distribution, where $\overline{z} = (1/N)\sum_{n=1}^{N} z_n$.

θ_d is a K-dimensional Dirichlet random vector; the parameter α is a K-dimensional vector each of whose elements are positive. Each trial is generated by again selecting from the Dirichlet random vector and repeating the entire process. Each z_n denotes a 1-of-K binary random vector with elements z_{nk} for $k = 1, \ldots, K$. $z_n, n = 1, \ldots, N$, are the LNS factors that induce an sEMG sequence. To describe the kth latent intention, the Gaussian parameters, mean vector μ_k, and covariance matrix Ω_k are fixed quantities. Given the quantities, a feature vector d_n of the data unit is drawn from the following distribution conditioned on z_n:

$$p(d_n|z_n, \mu_{1:K}, \Omega_{1:K}) = \prod_{k=1}^{K} N\left(\mu_k, \Omega_k\right)^{z_{nk}}. \tag{1}$$

A sequence of values of d_n over successive data units represents a trial. For applications, a class label c is drawn from the softmax distribution [28],

$$p(c|\overline{z}, \eta_{1:L}) = \exp\left(\eta_l^T \overline{z}\right) / \sum_{i=1}^{L} \exp\left(\eta_i^T \overline{z}\right) \tag{2}$$

where $\eta_{1:L}$ represents a set of L class coefficients; and each η_l is a K-dimensional vector whose elements are real values. Unknown parameters to be estimated are $\alpha, \mu_{1:K}, \Omega_{1:K}$, and $\eta_{1:L}$. Their optimal values are determined based on training trials. Section II-D will explain the optimization method. Once the model is established, sEMG-based classification is possible for future test trials.

This section introduced the concept of the generative process and relationship among parameters. From the next section, we describe each step sequentially: the feature extraction from sEMG signals in Section II-C, the hidden unknown variable optimization and estimation in Section II-D, and estimation of classification parameter in Section II-E.

C. sEMG Data Unit

Raw sEMG profiles can be windowed with or without overlap. Each window is regarded as a data unit. In a window, features are appropriately designated. Feature extraction relies on physical and neurophysiological conditions for a problem to be solved. The feature used in this work is the mean absolute value (MAV), which has commonly been used for muscle activation detection. The MAV is computationally simple and intuitive. It is computed as follows:

$$\text{MAV} = \frac{1}{M}\sum_{i=1}^{M} |x_i| \tag{3}$$

where x_i is a data point value at the ith time index, and M is the total number of data points in a window. Thus,

$$d_n = [\,\mathrm{MAV}_1 \quad \ldots \quad \mathrm{MAV}_H\,]^T \tag{4}$$

where the subscript indicates channel index assuming a trial records sEMG signals from H channels.

It should be noted that the sEMG data unit is the representation of a basic element of information. This work assumes that a sequence of sEMG units contains essential information encoded in the sEMG data from a trial. Other than the MAV, any possible combination of features is available [29], [30], and it has been shown that combinatory features are advantageous to attain high classification accuracy [31], [32]. However, this work restricts the use of other features because its primary aim is to show the feasibility of our approach not to find the best protocol for the highest classification accuracy.

D. Variational Inference

Finding the exact inference to compute the conditional distribution of the LNSs given the model is intractable. Instead, the method of variational inference approximation used in LDA is similarly applicable [24]. In the middle of the inference approximation, the factorized variational distribution of the latent variables is declared to be

$$q\left(\theta, z_{1:N}, |\gamma, \varphi_{1:N}\right) = q\left(\theta|\gamma\right) \prod_{n=1}^{N} q(z_n|\varphi_n). \tag{5}$$

Variational parameters γ and $\varphi_{1:N}$ are introduced; γ is a K-dimensional Dirichlet parameter; and each φ_n parameterizes a categorical distribution over K elements, where $\mathrm{E}[z_n] = \varphi_n$. Then, the minimization of the Kullback–Leibler (KL) divergence [33] between the factorized and the true posterior distributions is conducted using the variational expectation-maximization (EM) algorithm [34]. In the E step, the variational parameters are updated. The update rule of the variational parameter γ is identical to that of LDA [24], therefore,

$$\gamma^{\mathrm{new}} = \alpha + \sum_{n=1}^{N} \varphi_n. \tag{6}$$

Meanwhile, the update rule of the variational parameter φ_n is obtained by applying the technique introduced in [28] for the model, which includes a softmax classification, as follows:

$$\exp\left(\frac{1}{N}\eta_{lk} - (h^T\varphi_n)^{-1}h_k\right)\varphi_{nk}^{\mathrm{new}} = \kappa N(d_n|\mu_k,\Omega_k)\exp\left(\psi(\gamma_k) - \psi\left(\sum_{j=1}^{K}\gamma_j\right)\right) \tag{7}$$

where φ_{nk} is the kth element of $\varphi_n, h^T\varphi_n = \sum_{l=1}^{L}\prod_{n=1}^{N}(\sum_{k=1}^{K}\varphi_{nk}\exp(\frac{1}{N}\eta_{lk}))$ is a linear function of $\varphi_n, h = [h_1,\ldots,h_K]^T, \psi(\cdot)$ is a gamma function, and κ is a normalization factor.

In the M step, model parameters are estimated given the variational parameters. Gaussian parameters in the LNS are computed:

$$\mu_k^{\mathrm{new}} = \frac{\sum_{n=1}^{N}\varphi_{nk}d_n}{\sum_{n=1}^{N}\varphi_{nk}} \tag{8}$$

$$\Omega_k^{\mathrm{new}} = \frac{\sum_{n=1}^{N}\varphi_{nk}\left(d_n-\mu_k^{\mathrm{new}}\right)\left(d_n-\mu_k^{\mathrm{new}}\right)^T}{\sum_{n=1}^{N}\varphi_{nk}}. \tag{9}$$

Classification parameters $\eta_{1:L}$ can be estimated using the conjugate gradient [28], which is applied to

$$\sum_{t=1}^{T}\eta_{l_t}^T\overline{\varphi}_t - \log\left(\sum_{l=1}^{L}\prod_{n=1}^{N}\left(\sum_{k=1}^{K}\varphi_{tnk}\exp\left(\frac{1}{N}\eta_{lk}\right)\right)\right) \tag{10}$$

where $\overline{\varphi}_t = (1/N)\sum_{n=1}^{N}\varphi_{tn}$ at the tth trial. α can also be optimized [20]. However, practically, its value is fixed, for example, $\alpha = \left[\frac{1}{K},\ldots,\frac{1}{K}\right]^T$ uniformly.

The variational inference and the parameter estimation are repeatedly processed until the convergence is attained.

E. Classification

Once a model is learned, classification for future data can be performed. Given an unseen data, the learned model performs a variational inference on the data to identify variational parameters with LNSs estimated during training. Then, the same procedure as in [28] is applied, which results in a label selection such that

$$c^* = \arg\max_{l\in\{1,\ldots,L\}} E[\eta_l^T\overline{z}] = \arg\max_{l\in\{1,\ldots,L\}}\eta_l^T\overline{\varphi}. \tag{11}$$

For practical applications such as control of prosthetic devices or robotic arms, online or real-time classification is important [2], [22], [35]. To implement online classification, a decision is made per time window by modifying the classification rule as follows:

$$c_n^* = \arg\max_{l\in\{1,\ldots,L\}}\eta_l^T\varphi_n \text{ for the } n\text{th time window.} \tag{12}$$

Generally, increasing window length improves classification, while a longer processing time is required for a decision [35].

III. Experiments

A. Subject

Seven subjects volunteered for the experiments (mean $\pm$ SD age $= 27.4 \pm 2.96$ years). All of the participants were free of neuromuscular and musculoskeletal pathology. All of the subjects were given sufficient information about the purpose and procedures, and, before participation, informed consent was obtained from each subject. The KAIST Institutional Review Board approved the proposed experimental protocol of this study.

B. Experiment Design

Fig. 2 shows a list of the limb motions chosen in this study. The motions were chosen to intuitively represent all possible actions: wrist flexion/extension, radial/ulnar deviation, pronation/supination, and hand grip/open. The movement of opening

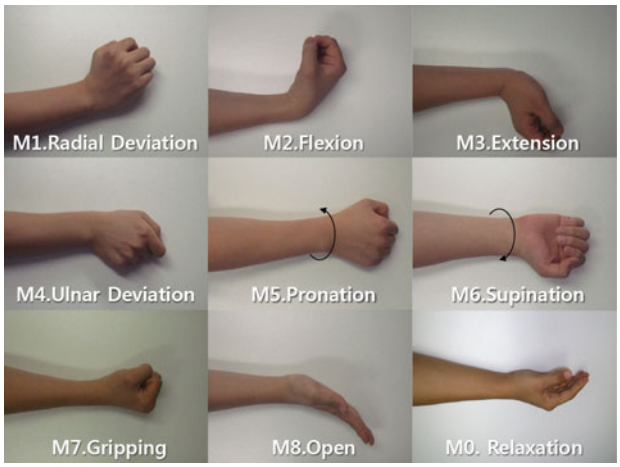

Fig. 2. Eight limb motions (M1–M8) with a relaxation pose (M0) for classification in this study.

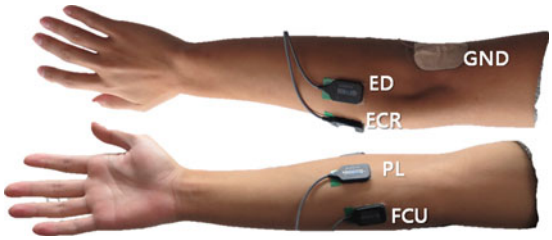

Fig. 3. Electrode locations chosen for this study. See also Table I.

TABLE I
ELECTRODE LOCATIONS ON THE FOREARM

Channel	Muscle	Function
1	Flexor Carpi Ulnaris (FCU)	Flexion, ulnar deviation (adduction) at wrist
2	Palmaris Longus (PL)	Flexion at wrist, tension at fingers
3	Extensor Carpi Radialis (ECR)	Extension, radial deviation (abduction) at wrist
4	Extensor Digitorum (ED)	Extension of fingers, extension at wrist

the hand also extends the fingers to distinguish it from the relaxation movement. The limb motions are easily executable, intuitive, and varied enough to be used for applications such as prosthetic or exoskeleton control [2], [21], [32], [35].

The actions are mainly governed by forearm muscles. The goal of this study is the classification of the nine wrist or finger postures, eight motions plus one relaxation posture, using the proposed model, and the model evaluation through the experimental results. A minimal number of electrodes were placed at sites such that interpreting the signal of different motions could be performed as accurately as possible across subjects. Fig. 3 shows the electrode locations selected considering particular muscles whose relevant functions contribute to the limb motions listed in Table I. Four electrodes were attached at each recording spot, as summarized in Table I. A fifth electrode was located on the upper arm as a reference to remove noise.

(a)

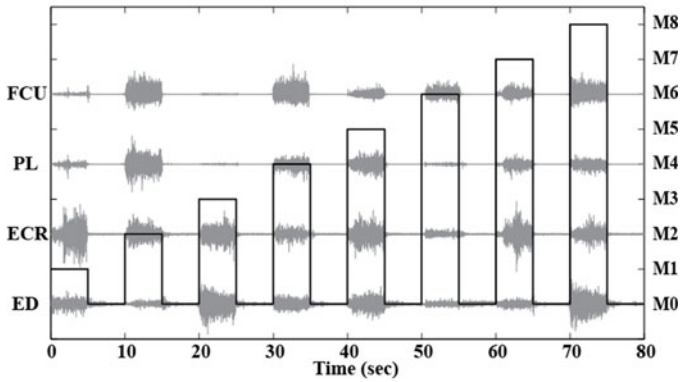

(b)

Fig. 4. (a) Experimental setup. (b) Experimental Procedure: black bold line represents the target motions from M0 to M8 over time and gray lines illustrate sEMG signals of the channels.

The subject was asked to sit comfortably in a chair with his right forearm lightly positioned on a horizontal plane with supports (Ergo Rest, USA). To allow the natural movement of the wrist, the wrist and hand were not constrained with any supports [see Fig. 4 (a)]. During movements, raw sEMG signals were measured using a commercial bipolar surface electrode and a filter-amplifier system (Bagnoli, Delsys Inc., USA).

C. Experimental Procedure

The experiments consisted of three sessions: pretest, a maximal voluntary contraction (MVC) check, and test sessions. During the pretest session, each subject took part in a familiarization session in which the subject became comfortable with the experimental equipment and practiced the experimental protocols. After the pretest session, maximum contraction values of each of the four muscles were recorded to be regarded as 100% MVC following the instructions on the computer screen. The subjects were asked to sequentially perform four wrist motions which exercised the maximum force of each muscle: radial deviation, flexion, extension, and ulnar deviation at MVC. It was requested that each wrist action be performed for 2 s.

In each experiment, each subject was asked to perform wrist motions sequentially at two distinctive muscular activation levels. It was very difficult to maintain a consistent contraction level; therefore, relatively low (20–30% MVC) and high (60–70%) activation level windows were designated. The activation level bar graph was shown on the screen during the experiment to help each subject maintain the level in real time. In each test session, the order of wrist motions was radial deviation, flexion, extension, ulnar deviation, pronation, supination, hand grasp, and hand open [see Fig. 4(b)] for 5 s. Relaxation posture was taken between any two sequential motions with the same interval. The motion sequence began with a relaxed natural posture of the wrist and hand. Each subject repeated the motion sequence five times at each muscular activation level. Therefore, five sessions per subject were recorded. The subject was allowed to relax between each session to avoid muscular fatigue, which could affect the myoelectric signal in the subsequent trials. The subject was not allowed to talk or move his body during the experiments, in order to avoid motion artifacts.

D. Signal Processing

The myoelectric signals were recorded simultaneously with a data acquisition system (NI 6221, National Instrument, USA), and were then sampled at 1 kHz. The myoelectric signals were band-pass filtered (5–450 Hz) using a zero phase fourth-order Butterworth filter; power line noise was rejected with an activated notch filter. The baselines of the myoelectric signals were shifted using mean values during the initial 10 s. Then, the myoelectric signals were normalized using MVC values. The static phase of each contraction was used for evaluation. The time window per data unit was set at 250 ms with a 50 ms window increment. The MAV feature was extracted in each window.

E. Modeling Condition and Motion Analysis

Various validation studies are conducted to assess the proposed model. First, the influence of the number of LNSs is examined. Second, the possibility of identifying the same motions without considering different activation levels is investigated in the combined activation level condition. Third, the performance of a generalized model across subjects is investigated. Finally, online classification using the proposed model is performed.

From the results, we analyze the sEMG strategy between high and low activation levels through the model in the combined activation level condition, sEMG strategy transition through the model in an online classification condition, and compare individual sEMG strategy through model in a cross subject condition.

IV. Strategy Analysis

This work assumes a motion's sEMG strategy can be indicated with respect to LNSs using the proposed model. The learned model describes a specific motion execution with a specified vector γ which expresses the relative contribution proportion of LNSs. kth LNS is expressed by its mean vector, μ_k, and covariance matrix, Ω_k, e.g., a Gaussian distribution. Hence,

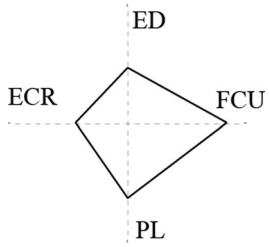

Fig. 5. Simple visualization of LNS that consists of the four-dimensional mean vector of the GMM for sEMG strategy analysis.

a characteristic of a specific motion in terms of the data units can be represented by a GMM as follow:

$$p(x) = \sum_{k=1}^{K} w_k N_k \tag{13}$$

where $w_k = \frac{\gamma_k}{\sum_{k=1}^{K} \gamma_k}$, $N_k = N(x; \mu_k, \Omega_k)$, γ_k is the kth element of γ which is estimated through the variational inference step using the specific motion data. Here, the random vector x represents MAVs relative to MVCs from the four electrodes.

To ease visual analysis and evaluation, the characteristic of a specific motion can be simply expressed by mean vector which is computed by

$$\overline{\mu}_s = \sum_{k=1}^{K} w_k \mu_k. \tag{14}$$

The mean vector indicates the representative magnitudes of muscular activations from the four electrodes as, for example, illustrated in Fig. 5. Therefore, it provides information on the sEMG strategy. Especially, when specific motions are executed by consistent muscular activations as in our cases, the mean vector describes the distribution of muscular activations intuitively.

For quantitative analysis, it is valid to measure similarity between sEMG strategies extracted from the probabilistic LNS space. This work considers the extended Jaccard distance which measure dissimilarity between two sample sets, and is complementary to the Jaccard coefficient [36] which is a variant of normalized inner product. Each mean vector of two motions in comparison is represented by (14) using a specific variational parameter γ inferred from each specific motion data in the LNS space. When $\overline{\mu}_a$ and $\overline{\mu}_b$ represent two mean vectors, the extended Jaccard distance is defined as follows:

$$J(\overline{\mu}_a, \overline{\mu}_b) = 1 - \frac{\overline{\mu}_a \cdot \overline{\mu}_b}{\overline{\mu}_{a2}^2 + \overline{\mu}_{b2}^2 - \overline{\mu}_a \cdot \overline{\mu}_b}. \tag{15}$$

As two sEMG strategies are more similar, the metric value becomes lower. The value is between 0 and 1. The original Jaccard index [37] is a similarity measure for binary features, but its extension in (15) is used with real-valued features. The Jaccard similarity is both scale and translation sensitive [36]; therefore, the overall scale and the relative contribution of individual elements of the mean vector can be taken into account to compare sEMG strategies as well.

TABLE II
OFFLINE INDIVIDUAL PATTERN CLASSIFICATION ACCURACY ACCORDING TO NUMBER OF LNSS (%): (a) HIGH, (b) LOW, AND (c) COMBINED ACTIVATION LEVEL CONDITION

	K	A	B	C	D	E	F	G	Average
(a) High	10	0.91± 0.03	0.87± 0.04	0.80± 0.09	0.86± 0.05	0.78± 0.11	0.92± 0.06	0.83± 0.03	0.85± 0.07
	20	0.91± 0.05	0.98± 0.02	0.88± 0.06	0.93± 0.04	0.82± 0.09	0.97± 0.05	0.88± 0.08	0.91± 0.07
	30	0.92± 0.02	0.92± 0.08	0.93± 0.06	0.92± 0.05	0.75± 0.06	0.96± 0.05	0.87± 0.04	0.90± 0.08
	40	0.91± 0.05	0.98± 0.02	0.92± 0.05	0.93± 0.04	0.78± 0.11	0.98± 0.02	0.88± 0.06	0.91± 0.08
	50	0.93± 0.04	1.00± 0.00	0.91± 0.07	0.95± 0.05	0.80± 0.10	0.93± 0.06	0.93± 0.04	0.92± 0.07
(b) Low	10	0.87± 0.12	0.77± 0.11	0.82± 0.05	0.83± 0.13	0.70± 0.18	0.81± 0.09	0.80± 0.06	0.80± 0.11
	20	0.90± 0.10	0.86± 0.02	0.87± 0.07	0.91± 0.12	0.71± 0.21	0.91± 0.07	0.87± 0.04	0.86± 0.11
	30	0.92± 0.06	0.86± 0.05	0.88± 0.05	0.92± 0.08	0.77± 0.16	0.93± 0.07	0.86± 0.11	0.88± 0.10
	40	0.90± 0.07	0.88± 0.12	0.92± 0.06	0.90± 0.07	0.73± 0.16	0.90± 0.06	0.87± 0.09	0.87± 0.10
	50	0.87± 0.04	0.82± 0.08	0.88± 0.08	0.95± 0.02	0.70± 0.17	0.89± 0.06	0.81± 0.09	0.84± 0.11
(c) Combined	10	0.72± 0.06	0.76± 0.08	0.79± 0.07	0.73± 0.07	0.65± 0.14	0.82± 0.08	0.79± 0.09	0.76± 0.09
	20	0.79± 0.06	0.81± 0.13	0.86± 0.06	0.83± 0.10	0.76± 0.13	0.89± 0.07	0.84± 0.05	0.83± 0.09
	30	0.85± 0.05	0.86± 0.13	0.90± 0.07	0.86± 0.12	0.75± 0.16	0.92± 0.04	0.85± 0.08	0.86± 0.10
	40	0.82± 0.07	0.85± 0.10	0.93± 0.05	0.87± 0.07	0.81± 0.05	0.91± 0.08	0.85± 0.10	0.87± 0.08
	50	0.80± 0.09	0.88± 0.06	0.93± 0.06	0.90± 0.07	0.77± 0.13	0.91± 0.06	0.85± 0.08	0.87± 0.08

TABLE III
ONLINE CLASSIFICATION ACCURACY ACCORDING TO NUMBER OF LNSS (%)

K	A	B	C	D	E	F	G	Average
30	0.80± 0.08	0.89± 0.07	0.87± 0.02	0.88± 0.04	0.73± 0.09	0.91± 0.03	0.82± 0.03	0.84± 0.07
40	0.80± 0.07	0.90± 0.08	0.86± 0.07	0.85± 0.05	0.74± 0.1	0.92± 0.03	0.80± 0.04	0.84± 0.08
50	0.77± 0.08	0.91± 0.03	0.85± 0.07	0.89± 0.04	0.73± 0.11	0.91± 0.07	0.83± 0.02	0.84± 0.08

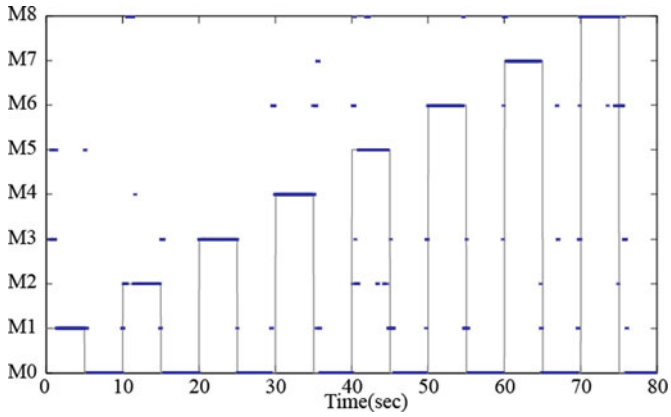

Fig. 6. Example of online classification over designated time window. Each dot indicates classification result at a specific instant interval.

V. RESULTS

A. Number of LNSs

As in [2], performance accuracy was measured based on leave-session-out cross validation. That is, the proposed model was trained with four sessions and tested with a remaining session. Average accuracy was obtained from five runs per test for each session. Table II shows accuracies of identifying the same motion intentions over the number of LNSs. Individual subjects are identified by letters A–G. In the high activation condition [Table II(a)], most of subjects achieved above 90% accuracy; a few had results of over 95%. In contrast, only a few cases achieved above 90% accuracy in the low activation condition [Table II(b)]. The model performance was poor with subject E in both conditions.

B. Combined Activation Level

To examine the influence of activation level on performance, myoelectric signals at both high and low activation levels were used together to train the model. For evaluation, leave-session-out cross validation was performed using all the data from both activation conditions. Table II(c) summarizes the results over the number of LNSs. With 30 and 40 LNSs, 86 and 87% accuracies were achieved on average, respectively. The classification accuracy was relatively lower than the single activation conditioned cases with the same number of LNSs probably because the model complexity is relatively higher.

C. Online Classification

To study the application of the model to online classification, simulation tests were conducted. Rather than training a model anew, the offline-trained model from the previous test was used. However, the online classification rule, as explained in Section II-D, was applied. Hence, each test session was classified online; that is, a classification result is an outcome per 250 ms time window with a 50 ms window increment. The results over the number of LNSs are summarized in Table III. Fig. 6 illustrates the online classification performance. False classification mainly occurred during motion transition periods.

D. Generalization Across Subjects

To study the model performance across subjects, the model was tested with leave-subject-out cross validation. That is, a specific subject's data was excluded during training, and the subject's data was used as test data. The model was trained using high activation conditioned electromyographic signals only, in order to clarify the LNSs by inferring each motion across subjects. The model can be regarded as a generalized one across subjects. Its overall performance for all of the LNSs is summarized in Table IV. On average, 84% accuracy was obtained with 50 LNSs ($K = 50$), although the generalized model across subjects performed less accurately than the subject-specific models overall.

TABLE IV
OFFLINE INDIVIDUAL PATTERN CLASSIFICATION ACCURACY WITH GENERALIZED MODEL ACROSS SUBJECTS ACCORDING TO NUMBER OF LNSS (%)

K	A	B	C	D	E	F	G	Average
30	0.72± 0.15	0.88± 0.08	0.65± 0.09	0.81± 0.05	0.63± 0.14	0.81± 0.04	0.81± 0.07	0.77± 0.09
40	0.78± 0.06	0.87± 0.05	0.76± 0.08	0.87± 0.04	0.76± 0.15	0.82± 0.08	0.81± 0.04	0.81± 0.07
50	0.81± 0.09	0.86± 0.05	0.83± 0.03	0.88± 0.08	0.73± 0.08	0.90± 0.05	0.81± 0.07	0.84± 0.06

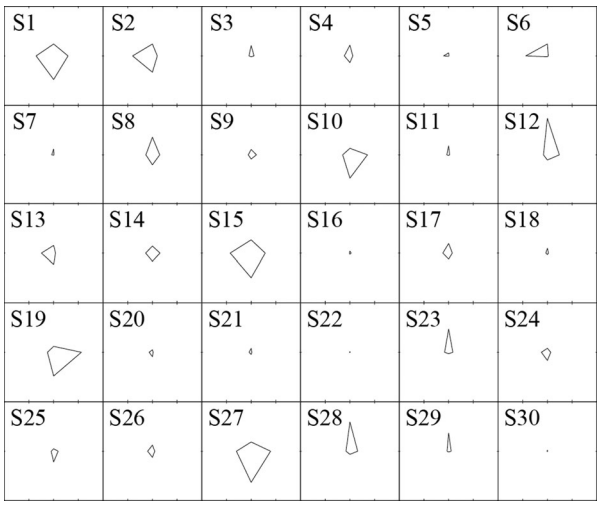

Fig. 7. Visualization of each LNS in the combined activation level conditioned model. The LNSs are labeled from S1 to S30 (the label order is meaningless).

VI. DISCUSSION

A. Number of LNSs

Although subject-specific performance is different, the classification accuracy over the number of LNSs tends to increase until some optimal number of LNSs, after which it slowly decreases due to model overfitting. We analyzed and selected the optimal number of LNSs overall from the individual results. Accuracies were only obtained for up to 50 LNSs because computational complexity becomes much higher when there are more than 50 LNSs.

In a comparison of the activation levels, the high activation conditioned accuracy was found to be higher than the low activation conditioned accuracy. High activation seems to better clarify each intended motion. Above 20 LNSs ($K > 20$) note that there is an appropriate choice to obtain reasonable overall accuracies of at least 91% for high contraction level and 86% for low contraction level across all subjects.

B. Combined Activation Conditioned Model Analysis

A trained model incorporates LNSs that describe activation patterns. To demonstrate analyzing a trained model in detail, this section uses the combined activation conditioned model obtained from subject D's data as an example. From this model, the estimated LNSs when $k = 30$ are illustrated in Fig. 7.

TABLE V
MAJOR INFLUENTIAL LNSS WITH WHOLE ACTIVATION CONDITIONED MODEL OF SUBJECT D

Motion	Activation level	1st	2nd	3rd	4th
M1	High	S13 (0.97)			
	Low	S20 (0.95)			
M2	High	S19(0.72)	S10 (0.25)		
	Low	S25 (0.97)			
M3	High	S6 (0.97)			
	Low	S5 (0.97)			
M4	High	S8 (0.85)	S28 (0.12)		
	Low	S11 (0.97)			
M5	High	S8 (0.93)	S17 (0.04)		
	Low	S18 (0.49)	S21 (0.35)	S9 (0.13)	
M6	High	S14 (0.86)	S26 (0.06)	S8 (0.05)	
	Low	S9 (0.67)	S18 (0.29)		
M7	High	S10 (0.32)	S8 (0.27)	S1 (0.19)	S2 (0.18)
	Low	S25 (0.60)	S24 (0.37)		
M8	High	S12 (0.97)			
	Low	S29 (0.95)			
M0	High	S22 (0.54)	S30 (0.42)		
	Low	S22 (0.63)	S16 (0.21)	S30 (0.11)	

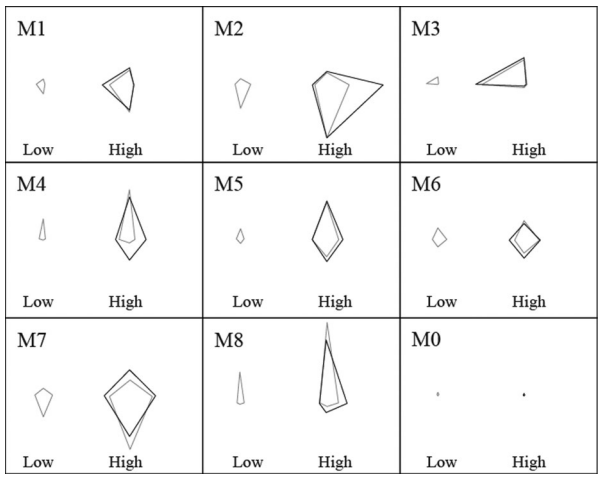

Fig. 8. Comparison between the mean vectors of low (thin line) and high (thick) activation conditions per motions extracted from the combined activation conditioned model. And, for clarity, scale-adjusted mean vectors of low activation conditions are overlapped with them of high activation conditions.

Relative contribution proportion of LNSs per motion is obtained by averaging γ values estimated through variational inference. Table V summarizes the most influential LNSs which cover at least 95% of the total proportions in which they contributed. The relative contribution proportions are also indicated in parentheses in Table V. It is clearly shown that relatively large scaled LNSs are mainly contributed for motions with high activation levels. Meanwhile, relatively small scaled LNSs dominates the representation of motions with low activation levels. With the obtained accuracy, the learned model constructs the LNS space, which characterizes both low and high activation conditioned motions.

Fig. 8 visualizes each mean vector per each motion in both activation level cases. The mean vectors of low and high activation conditions are drawn in thin and thick lines, respectively.

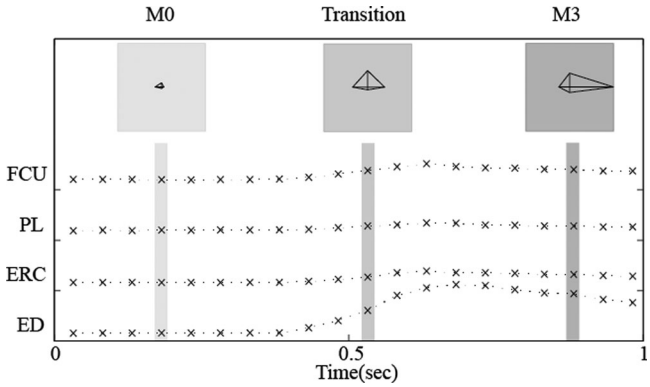

Fig. 9. Example of motion transition over time in online classification performance. Dot and cross represent instant features of each muscle, and gray boxes depict the dataset and related mean vector visualization.

In addition, for easy comparsion, the mean vector scales of low activation conditioned cases are matched and drawn overlapped with the high activation condition cases in Fig. 8. sEMG strategies between low and high activation conditioned cases are clearly distinguished in terms of the amplitude of the mean vector. However, the relative distribution of the mean vectors seem comparable between the two cases per each motion. Motions M1, M3, M5, M6, M7, M8, and M0 demonstrate quite consistent results between the two activation conditions. Except for motions M2 and M4, the motions amplify the mean vector scales maintaining a relative activation pattern over the muscles. In M2 and M4, the relative distributional difference between two activation conditions other than the scale change is visually observed further relative to the other motions. At M2 (flexion), LNS of low activation level (S25) is dominant on the downward element (PL), but the LNS at high activation level, a combination of S19 and S10, indicates relatively significant rightward element (FCU) increment. This can be explained that more cocontractions were activated to generate higher activation. Motion M4 (deviation) case can also be similarly explained. Upward directional element (ED) is generated dominantly in low activation condition, but as activation level increases, other muscular activations are also significantly increased.

C. sEMG Strategy Transition

As a typical example, Fig. 9 illustrates the time flow of the online performance around the transition period from relaxed posture (M0) to motion M3. The mean vectors at selected windows are indicated. In the middle of the transition, the mean vector is shaped between motions M0 and M3. The mean vector could lead to wrong classification at that instant; however, it may be able to explain transient muscular activation between motions M0 and M3. That is to say, the transient muscular activations do not match specified sEMG strategies well; hence, false classifications are frequently seen during the transition. The proposed model allows continuous tracking of sEMG strategies or influential LNSs over time. Thus, it can identify the dynamics of sEMG strategies in a spatial representation. The information on proportional changes of sEMG strategies from one motion to another may extend possible applications to those beyond discrete classification.

To enhance motion classification accuracy, it is possible to use a postprocessing method such as a majority vote [35]. However, this work is intended to emphasize the primary characteristic of the proposed model, which is its ability to capture the stream of motion change.

D. Subject's Generalized Model Analysis

To analyze the structure of the LNS space of a generalized model across subjects, this section uses a model trained with the other subjects' data to test subject F. The performance accuracy of this case is shown in Table III and is 90% when $K = 50$. Under the model's accuracy, the similarity measure between two motions with respect to LNSs as in (15) is applied, and its result is visualized as similarity matrix in Fig. 10. As two motions are more similar in strategy, the pixel color is closer to red. For easy comparison, the similarity matrix is drawn with respect to the between-subject similarity across motions [Fig. 10(a)] and the between-motion similarity across subjects [Fig. 10(b)] separately. Fig. 10(a) visually shows motions are generally distinguishable across subjects. In addition, some reddish areas indicate similar strategies are shared between different subjects. Even within a subject, some different motions are relatively similar. For example, subject E shares similarity between M5 and M6. In Fig. 10(b), motions M2, M3, M6, and M0 turn out to be executed mostly similarly over subjects. A more detailed observation is possible. For example, in M2 and M3, subject G has a clearly different strategy from the others. The rest posture M0 is relatively well distinguished from other motions. This seems due to the activation scale. Fig. 10(c) visualizes hierarchical cluster analysis which more effectively demonstrates identical observations from Fig. 10(a) and (b).

To see how the similarity or dissimilarity is expressed in the LNS space, Fig. 11 demonstrates some examples of the comparison of the mean vectors extracted from the model to describe the same motion executed by different subjects. As shown in Fig. 11(a), at M2 (flexion), subject G's sEMG strategy represented by a mean vector is the most distinguished from the others, and subject C's one is the second most distinguished. Those two subjects have lower downward elements (PL) as well as lower activation scales. In Fig. 11(b), while executing M3(extension), most subjects' sEMG strategies possessed greater leftward elements (ECR) than rightward elements (FCU) except subject G. Fig. 11(b) demonstrates examples of describing different motions of a subject in the LNS space. As indicated in Fig. 10, some motions are similar in their mean vectors. For example, M5 and M6 are quite similar for subject E, meanwhile M1, M2, and M5 are quite similar for subject F. This implies that those motions are hard to distinguish during classification. In addition, it is visually recognized that subject F tends to activate the PL muscle while executing various motions. On the other hand, subject E uses the PL muscle much less than subject E. These observations demonstrate that the model captures subject-specific characteristics of motion execution.

Overall, including the unseen cases here, the trained model describes shared motion execution strategies between subjects

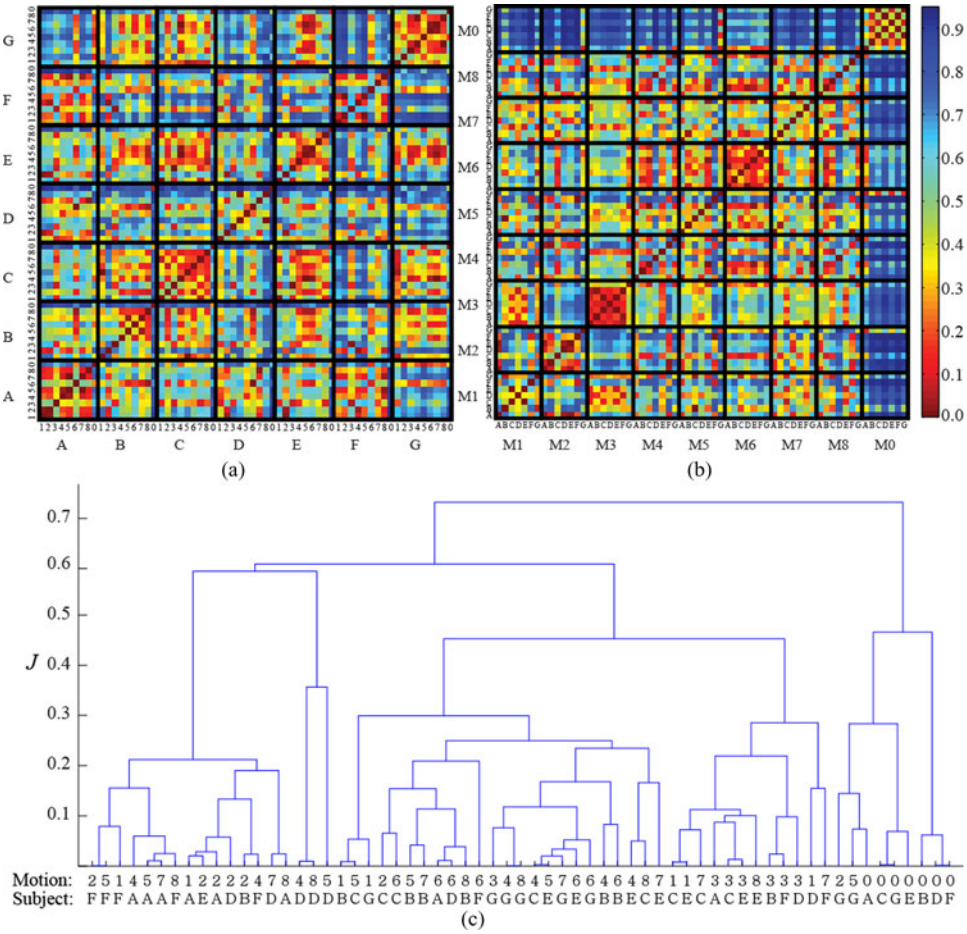

Fig. 10. Similarity matrices based on extended Jaccard distance, J, (a) between subjects across motions and (b) between motions across subjects. Two motions are more similar when the pixel color is closer to red. (c) Hierarchical cluster analysis. Motions are clustered based on their similarity.

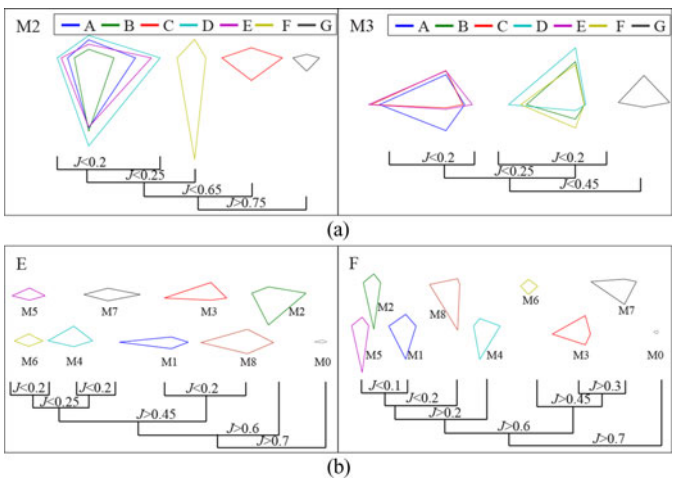

Fig. 11. (a) Comparison between the mean vectors which infer the same motion per subjects extracted from the generalized model: (left) M2 and (right) M3. Similarity values are indicated below. (b) Comparison between the mean vectors which infer various motions executed by the subject extracted from the generalized model: (left) subject E and (right) subject F.

with respect to LNSs as well as different strategies even for the same executed motion. In addition, a particular motion or comparison between particular motions or particular subjects can also be characterized with respect to the LNSs. The results indicate that the proposed model as a single coherent model is able to incorporate diverse strategies and signify complicated correlations of various motions in the LNS space as well.

E. Remarks

This section summarizes some nontrivial remarks. The proposed model not only attained high accuracy for subject-specific performance but also demonstrated its potential for use in the design of a generalized classification system across subjects. Furthermore, the model can be used to analyze characteristics of individual motion executions in the LNS space. The spatial LNS representation is valuable for not only motion classification but also motion-specific or subject-specific characterization and analysis.

Our approach did not require an explicit optimal feature extraction procedure. While training the model, optimal features were extracted implicitly and automatically. Furthermore, the model did not rely on prior knowledge of model parameters. During online processing, continuous tracking of major influential LNSs, or sEMG strategies was possible unlike other traditional approaches. The online monitoring will be very effective to extend to other electromyographic control applications.

The output response of the current model was designed for classification problems using the softmax function. However, the output response model can be extended or modified for any other application. Appropriate selection of the output response model would make it possible to generate control signals based on an entire probability distribution over LNSs rather than discrete classification decisions. Further investigation on other response models is expected.

Previously, Bayesian models such as HMM and GMM [21], [22] have been applied for electomyographic control. The HMM- or GMM-based approaches require a number of models equivalent to the number of classification labels. Then, a label is decided on to correspond to the model that attains the maximum likelihood value given the data. Different from these approaches, the proposed model includes a dimension of the classification parameter that relies on the number of labels; the natural description of the proposed model remains unchanged.

During training, the proposed model relies on the variational EM algorithm for optimization. EM's convergence speed is generally known to be sensitive to parameter initialization. To attain quick and stable convergence, an efficient initialization method such as an iterative point refinement algorithm [38] may be effective.

There are still unexplored issues such as the selection of a time window length [35] and application of any other features beyond MAV [29], [30]. The optimized number of LNSs varied from subject to subject. The subject-dependent issue should also be further investigated.

VII. Conclusion

This paper presented information on the progress of generative model-based electromyographic control. The proposed hierarchical Bayesian model offers intuitive signal processing and effective analysis; these are very useful during implementation. Furthermore, the generative model automatically determines LNSs, which are key components of classification. Therefore, users do not need to find optimal features separately. This paper has also demonstrated that the proposed model can reflect various muscular activation patterns across subjects as well as represent subject-specific characteristics of muscular activities. Such potential functions will promote the feasibility of the proposed model for applications. Even though further exploration is required, this work proposes that the hierarchical Bayesian model is a natural, intuitive, and efficient means for myoelectric assistive device interface or control development.

Acknowledgment

The authors would like to thank J. Cho for technical discussion and T. Morse for editorial assistance, and appreciate the valuable comments from anonymous reviewers.

References

[1] T. S. Saponas, D. S. Tan, D. Morris, R. Balakrishnan, J. Turner, and J. A. Landey, "Enabling always-available input with muscle-computer interfaces," in *Proc. 22nd Annu. ACM Symp. User Interface Softw. and Technol.*, Victoria, British Columbia, Canada, Oct. 2009, pp. 167–176.

[2] P. Shenoy, K. J. Miller, B. Crawford, and R. P. N. Rao, "Online electromyographic control of a robotic prosthesis," *IEEE Trans. Biomed. Eng.*, vol. 55, no. 3, pp. 1128–1135, Mar. 2008.

[3] S. Bitzer and P. van der Smagt, "Learning EMG control of a robotic hand: Towards active prostheses," in *Proc. IEEE Int. Conf. Robot. Autom.*, Orlando, Florida, May 2006, pp. 2819–2823.

[4] K. H. Ha, H. A. Varol, and M. Goldfarb, "Volitional control of a prosthetic knee using surface electromyography," *IEEE Trans. Biomed. Eng.*, vol. 58, no. 1, pp. 144–151, Jan. 2011.

[5] F. H. Y. Chan, Y.-S. Yang, F. K. Lam, Y.-T. Zhang, and P. A. Parker, "Fuzzy EMG classification for prosthesis control," *IEEE Trans. Rehabil. Eng.*, vol. 8, no. 3, pp. 305–311, Sep. 2000.

[6] K. Kiguchi, T. Tanaka, and T. Fukuda, "Neuro-fuzzy control of a robotic exoskeleton with EMG signals," *IEEE Trans. Fuzzy Syst.*, vol. 12, no. 4, pp. 481–490, Aug. 2004.

[7] E. Cavallaro, J. Rosen, J. C. Perry, S. Burns, B. Hannaford *et al.*, "Hill-based model as a myoprocessor for a neural controlled powered exoskeleton arm – parameters optimization," in *Proc. IEEE Int. Conf. Robot. Autom.*, Barcelona, Spain, 2005, pp. 4525–4530.

[8] C. Fleischer and G. Hommel, "A human-exoskeleton interfaces utilizing electromyography," *IEEE Trans. Robot.*, vol. 24, no. 4, pp. 872–882, Aug. 2008.

[9] Z. O. Khokhar, Z. G. Xiao, and C. Menon, "Surface EMG pattern recognition for real-time control of a wrist exoskeleton," *BioMed. Eng. Online*, vol. 9, no. 41, 2010.

[10] P. K. Artemiadis and K. J. Kyriakopoulos, "A switching regime model for the EMG-based control of a robot arm," *IEEE Trans. Syst., Man, and Cybern. B*, vol. 41, no. 1, pp. 53–63, Feb. 2011.

[11] Y. Chae, C. Choi, J. Kim, and S. Jo, "Noninvasive sEMG-based control for humanoid robot teleoperated navigation," *Int. J. Precis. Eng. Manuf.*, vol. 12, no. 6, pp. 1105–1110, 2011.

[12] F. Tenore, A. Ramos, A. Fahmy, S. Acharya, R. Etienne-Cummings, and N. V. Thakor, "Towards the control of individual fingers of a prosthetic hand using surface EMG signals," in *Proc. IEEE Annu. Int. Conf. Eng. Med. Bio. Sci.*, Lyon, France, Aug. 2007, pp. 6145–6148.

[13] S. Kwon and J. Kim, "Real-time upper limb motion estimation from surface electromyography and joint angular velocities using an artificial neural network for human-machine cooperation," *IEEE Trans. Inform. Tech. Biomed.*, vol. 15, no. 4, pp. 522–520, Jul. 2011.

[14] K. Kiguchi, T. Tanaka, and T. Fukuda, "Neuro-fuzzy control of a robotic exoskeleton with EMG signals," *IEEE Trans. Fuzzy Syst.*, vol. 12, no. 4, pp. 481–490, Aug. 2004.

[15] A. V. Hill, "The heat of shortening and the dynamic constants of muscle," in *Proc. R. Soc. Lond. B*, 1938, vol. 126, no. 843, pp. 136–195.

[16] B. A. Garner and M. G. Pandy, "Estimation of musculotendon properties in the human upper limb," *Ann. Biomed. Eng.*, vol. 31, pp. 207–220, 2003.

[17] D. G. Lloyd and T. F. Besier, "An EMG-driven musculoskeletal model to estimate muscle forces and knee joint moments in vivo," *J. Biomech.*, vol. 36, pp. 765–776, 2003.

[18] M. A. Oskoei and H. Hu, "Myoelectric control systems-a survey," *Biomed. Signal Process Control*, vol. 2, pp. 275–294, 2007.

[19] T. D. Sanger, "Bayesian filtering of myoelectric signals," *J. Neurophysiol.*, vol. 97, pp. 1839–1845, 2007.

[20] N. Bu, M. Okamoto, and T. Tsuji, "A hybrid motion classification approach for EMG-based human-robot interfaces using Bayesian and neural networks," *IEEE Trans. Robot.*, vol. 25, no. 3, pp. 502–511, Jun. 2009.

[21] A. D. C. Chan and K. B. Englehart, "Continuous myoelectric control for powered prostheses using hidden Markov models," *IEEE Trans. Biomed. Eng.*, vol. 52, no. 1, pp. 121–123, Jan. 2005.

[22] Y. Huang and K. B. Englehart, "A Gaussian mixture model based classification scheme for myoelectric control of powered upper limb prostheses," *IEEE Trans. Biomed. Eng.*, vol. 52, no. 11, pp. 1801–1811, Nov. 2005.

[23] D. M. Blei, "Probabilistic topic models," *Commun. ACM*, vol. 55, no. 4, pp. 77–84, 2012.

[24] D. Blei, A. Ng, and M. Jordan, "Latent Dirichl *et al*. location," *J. Mach. Learn. Res.*, vol. 3, pp. 993–1022, 2003.

[25] D. Blei and J. McAuliffe, "Supervised topic models," in *Proc. Neural Inf. Process. Syst.*, 2007, vol. 21.

[26] E. A. Clancy and N. Hogan, "Probability density of the surface electromyogram and its relation to amplitude detectors," *IEEE Trans. Biomed. Eng.*, vol. 46, no. 6, pp. 730–739, Jun. 1999.

[27] N. Hogan and R. W. Mann, "Myoelectric signal processing: Optimal estimation applied to electromyography—Part II: Experimental demonstration of optimal myoprocessor performance," *IEEE Trans. Biomed. Eng.*, vol. BME-27, no. 7, pp. 396–410, Jul. 1980.

[28] C. Wang, D. Blei, and L. Fei-Fei, "Simultaneous image classification and annotation," in *Proc. Comput. Vision Pattern Recog.*, 2009.
[29] M. Zardoshti-Kermani, B. C. Wheeler, K. Badie, and R. M. Hashemi, "EMG feature evaluation for movement control of upper extremity prostheses," *IEEE Trans. Rehabil. Eng.*, vol. 3, no. 4, pp. 324–333, Dec. 1995.
[30] D. Tkach, H. Huang, and T. A. Kuiken, "Study of stability of time-domain features for electromyographic pattern recognition," *J. Neuroeng. Rehabil.*, vol. 7, no. 21, 2010.
[31] U. M. Fayyad, C. A. Reina, and P. S. Bradley, "Initialization of iterative refinement clustering algorithms," in *Proc. Int. Conf. Knowl. Discovery Data Mining*, 1998.
[32] J.-U. Chu, I. Moon, and M.-S. Mun, "A real-time EMG pattern recognition system based on linear-nonlinear feature projection for a multifunction myoelectric hand," *IEEE Trans. Biomed. Eng.*, vol. 53, no. 11, pp. 2232–2239, Nov. 2006.
[33] S. Kullback and R. A. Leibler, "On information and sufficiency," *Ann. Math. Stat.*, vol. 22, no. 1, pp. 79–86, 1951.
[34] A. P. Dempster, N. M. Laird, and D. B. Rubin, "Maximum likelihood from incomplete data via the EM algorithm," *J. Roy. Stat. Soc. B*, vol. 39, no. 1, pp. 1–38, 1977.
[35] K. Englehart and B. Hudgins, "A robust, real-time control scheme for multifunction myoelectric control," *IEEE Trans. Biomed. Eng.*, vol. 50, no. 7, pp. 848–854, Jul. 2003.
[36] J. Ghosh and A. Strehl, "Similarity-based text clustering: A comparative study," in *Grouping Multidimensional Data*. Berlin: Springer, 2006, pp. 73–97.
[37] P. Jaccard, "Étude comparative de la distribution florale dans une portion des Alpes et des Jura," *Bulletin de la Société Vaudoise des Sci. Naturelles*, vol. 37, pp. 547–579, 1901.
[38] P. S. Bradley and U. M. Fayyad, "Refining initial points for K-means clustering," Microsoft Res. Tech. Rep. MSR-TR-98–36, 1998.

Hyonyoung Han received the B.S., M.S., and Ph.D. degrees from the Department of Mechanical Engineering, Korea Advanced Institute of Science and Technology (KAIST), Daejeon, Korea, in 2005, 2007, and 2012, respectively.

He is currently a Postdoctoral Researcher with the Department of Computer Science, KAIST. His research interests include physical human robot interaction, health monitoring, and bioinstrumentation.

Sungho Jo (M'09) received the B.S. degree from the School of Mechanical and Aerospace Engineering, Seoul National University, Korea, in 1999, and the M.S. degree in Mechanical Engineering and the Ph.D. degree in Electrical Engineering and Computer Science both from the Massachusetts Institute of Technology (MIT), Cambridge, USA, in 2001 and 2006, respectively.

While pursuing the Ph.D. degree, he was with the Computer Science and Artificial Intelligence Laboratory and the Laboratory for Information Decision and Systems. From 2006 to 2007, he was a Postdoctoral Researcher with the MIT Media Lab. Since December 2007, he has been with the Department of Computer Science, Korea Advanced Institute of Science and Technology, Daejeon, Korea, where he is currently an Associate Professor. His research interests include brain-machine interface, muscle-computer interface, and wearable computing.